Array Calibration for CDMA Smart Antenna Systems

Mun Geon Kyeong, Hyung Geun Park, Hyun Seo Oh, and Jae Ho Jung

In this paper, we investigate array calibration algorithms to derive a further improved version for correcting antenna array errors and RF transceiver errors in CDMA smart antenna systems. The structure of a multi-channel RF transceiver with a digital calibration apparatus and its calibration techniques are presented, where we propose a new RF receiver calibration scheme to minimize interference of the calibration signal on the user signals. The calibration signal is injected into a multi-channel receiver through a calibration signal injector whose array response vector is controlled in order to have a low correlation with the antenna response vector of the receive signals. We suggest a model-based antenna array calibration to remove the antenna array errors including mutual coupling errors or to predict the element patterns from the array manifold measured at a small number of angles. Computer simulations and experiment results are shown to verify the calibration algorithms.

Keywords: Array calibration, antenna array errors, RF transceiver error, CDMA, smart antennas, multi-channel RF transceiver, model based antenna array calibration.

Manuscript received Nov. 11, 2003; revised Oct. 13, 2004.

Mun Geon Kyeong (phone: +82 42 860 1150, email: mgk@etri.re.kr), Hyung Geun Park (email: hgpark@etri.re.kr), and Jae Ho Jung (email: jhjung@etri.re.kr) are with Mobile Telecommunication Research Division, ETRI, Daejeon, Korea.

Hyun Seo Oh (email: hsoh5@etri.re.kr) is with Telematics Research Division, ETRI, Daejeon, Korea.

I. Introduction

A basestation system using an adaptive array antenna is expected to increase its maximum range and capacity due to an improved antenna gain and the reduction of interference from other spatially separated users [1], [2]. Beamforming algorithms often assume that the array antenna has no errors and that the multi-channel transceiver has an identical transfer function. However, the spatial signature of the baseband receive/transmit signal is significantly different from that of the RF receive/transmit signal. This is because the transfer functions of the RF transceivers are different from each other. Therefore, knowledge of such errors is essential for the beamforming algorithms using the spatial signature of the RF receive/transmit signals. Some adaptive algorithms such as the recursive least square and least mean square algorithms are not sensitive to the errors induced in the uplink beamforming. Nevertheless, we need an accurate estimate of the transfer function of the multi-channel transceiver because the spatial signature of the RF receive signal at the antenna array is essential in the downlink beamforming [3], [4]. The performance of a smart antenna system can also be degraded by antenna array errors such as mutual coupling between antenna elements and scattering by the antenna structure or nearby scatterers [5]. Since a basestation system with three sectors has to scan one 120° sector angle, the spacing between antenna elements should be small to eliminate the grating lobe where contrarily the mutual coupling error becomes larger. The antenna array errors will distort the array beam pattern and result in an increased sidelobe level which means an increased interference to other users and reduced array gain.

Algorithms to calibrate both antenna array and the receiver simultaneously by using an external source transmitting

calibration signals at known or unknown directions have been developed for other array antenna system applications [6]-[8]. However, it is difficult to directly use these algorithms for smart antenna applications because the received signals at the basestation antenna array have many multipath components with different angles of arrival (AoAs). In particular, since the antenna array error is a function of frequency, the array errors at the transmit frequency cannot be estimated from the received signals in the frequency division duplex smart antenna systems. Therefore, it is more advantageous to calibrate the antenna array and transceiver separately [9].

For an RF transceiver calibration, the calibration should be done during a system operation called 'on-line calibration' because the transfer function can change with temperature and humidity. In particular, the transfer function of a receiver is a function of the receiver gain instantaneously being changed by the automatic gain control. A blind calibration algorithm using the minimum mean square error algorithm was proposed [10]. It requires only the receive/transmit signals and does not require any calibration signal for estimating the transfer function. Usually, the transfer function is estimated by injecting a known calibration signal into each transceiver via passive RF components such as a power splitter (or switch) and directional coupler, whose transfer functions are measured before system installation [9]. The calibration signal should be injected into the multi-channel receiver with time intervals short enough to track the change of the receiver gain, and its power should be small enough not to be an interference to the user signals received through the antenna array. In this paper, a method of injecting the calibration signal into a multi-channel receiver is proposed to reduce the interference to the user signals. Discussions on a multi-channel transmitter calibration for the CDMA smart antenna system are also provided.

For the antenna array calibration, an 'off-line calibration' estimating the error before system installation is more desirable because the characteristics of the antenna hardly changes. Several model-based antenna array calibration techniques were proposed and experimentally evaluated [11], [12]. They assumed that the mutual coupling error is independent of angle under a single-mode assumption, meaning that the shape of the current distribution at the antenna elements does not change with the beam directions. Thus, the antenna array errors can be modeled as

$$\mathbf{b}(\theta) = f(\theta)\mathbf{M}\mathbf{a}(\theta), \tag{1}$$

where $\mathbf{b}(\theta)$ and $\mathbf{a}(\theta)$ denote the response vectors of the practical antenna array and ideal isotropic antenna array for angle θ, respectively. The isolated element pattern assumed to be same for all elements in this paper is $f(\theta)$. The error matrix $\mathbf{M}$ includes unequal feeder transfer functions as well as the mutual coupling. The array model in (1) will not be valid if the modeling errors such as the scattering by the edge of the ground plate or by nearby scatterers are negligible [13]. The effect of nearby scatterers can be reduced by a careful placement of the antenna array, and the effect of the finite ground plate can also be reduced by just extending the plate or rolling the edge [14]. The mutual coupling matrix is estimated by a Fourier transformation of the measured element patterns in [11]. This has some limitations in that it requires an isolated element pattern and cannot be directly applied for an antenna array with an element spacing smaller than 0.5 wavelength. The simple least square method was used to estimate the array error matrix [12],

$$\hat{\mathbf{M}} = \mathbf{B}\mathbf{A}_f^H(\mathbf{A}_f\mathbf{A}_f^H)^{-1}, \tag{2}$$

where $\mathrm{B}=[\mathbf{b}(\theta_1), \mathbf{b}(\theta_2),\ldots,\mathbf{b}(\theta_N)]$ and $\mathbf{A}_f=[f(\theta_1)\mathbf{a}(\theta_1), f(\theta_2)\mathbf{a}(\theta_2),\ldots,f(\theta_N)\mathbf{a}(\theta_N)]$ denote the measured manifold of the practical antenna array and the calculated manifold of the ideal antenna array, respectively. The number of collected array response vectors N in $\mathbf{B}$ and $\mathbf{A}_f$ should be larger than the number of elements in the array in order to avoid the matrix singularity problem. As can be seen in (2), the least square solution also requires the isolated element pattern. It also requires the rotation center of the array, which is difficult to accurately know in a practical antenna measurement range because the phase center of $\mathbf{a}(\theta_i)$ is determined by the rotation center.

The rest of the paper is organized as follows. In section II, the RF transceiver calibration technique is described. In section III, the model-based array antenna calibration is presented and evaluated by simulation and experiment. Section IV offers concluding remarks.

II. RF Transceiver Calibration

1. RF Transceiver Calibration for CDMA Smart Antenna Systems

A block diagram of the multi-channel RF transceiver for a CDMA smart antenna system is shown in Fig. 1, where the RF transceiver depicts all RX/TX modules except the array antenna, which can generate various unbalanced errors among the channels. For the multi-channel receiver calibration, an RF calibration signal can be injected into the multi-channel receiver in two ways. One way is to inject the calibration signal into all the receivers simultaneously ('simultaneous calibration'), and the other is to inject it into each receiver sequentially ('sequential calibration'). To estimate the transfer function of all the receivers in a predetermined calibration period, the sequential calibration has to estimate a transfer function of each receiver for the time duration, which is M

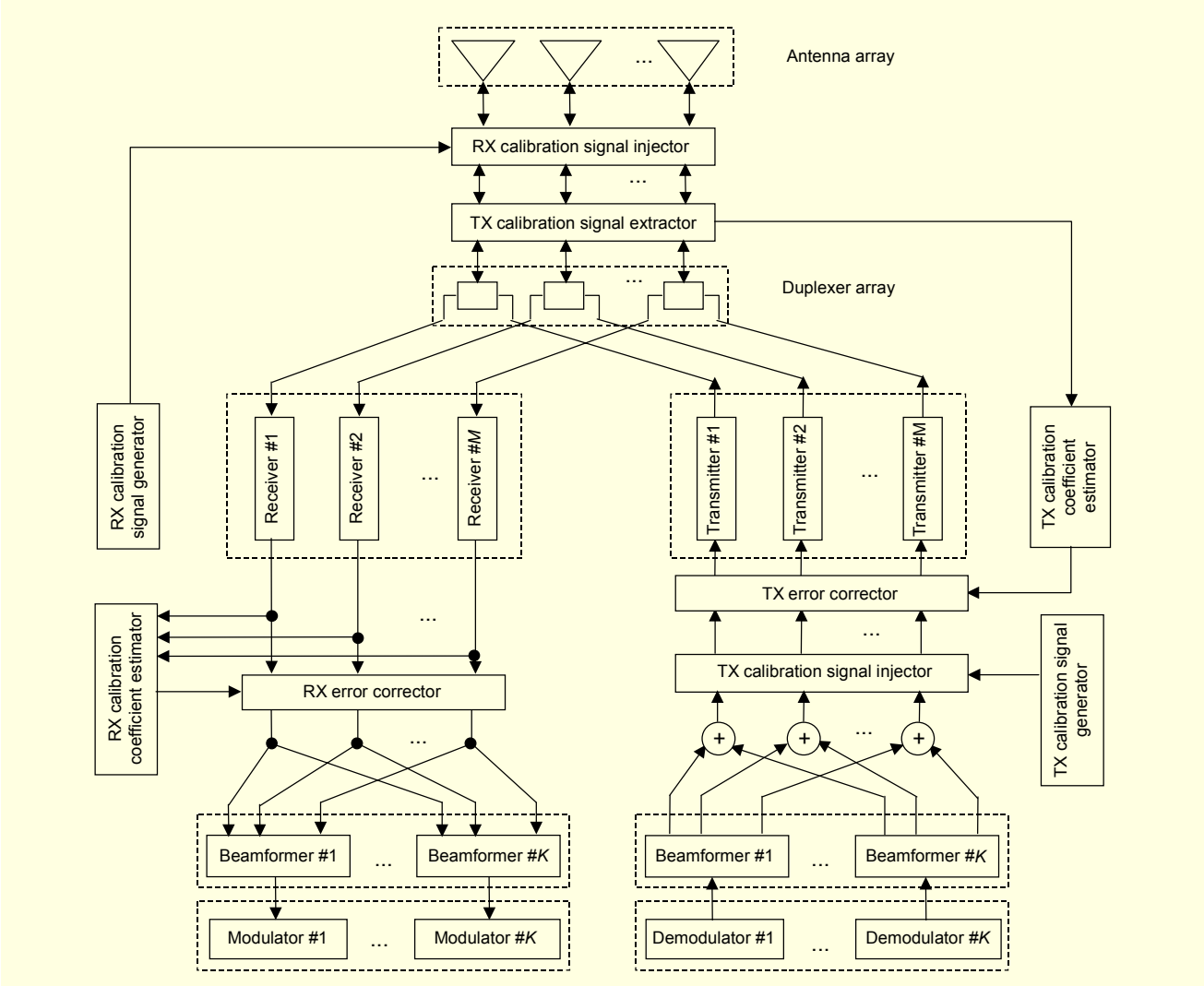

Fig. 1. Block diagram of the multi-channel RF transceiver.

times smaller than the calibration period. M is the number of radiating elements in the antenna array. Therefore, the calibration signal power for the sequential calibration should be M times larger than that for the simultaneous calibration to estimate the transfer function with the same accuracy.

For the simultaneous calibration, the RF calibration signal is divided into M channels and simultaneously injected into the multi-channel receiver. The RF calibration signal is down-converted by the multi-channel receiver, and the output snapshot vector of the multi-channel receiver $\mathbf{y}$ can then be defined as

$$\mathbf{y}(t) = \mathbf{H}_r \left[\sum_i \mathbf{a}(\theta_i) s_i(t) + \boldsymbol{\alpha} c(t) \right], \tag{3}$$

where $s_i(t)$ represents the received signal of the i-th user and $c(t)$ the calibration signal. The array response vector of the i-th user signal coming from direction θ_i can be expressed as column vector $\mathbf{a}(\theta_i) = [1 \quad e^{jkd\sin(\theta_i)} \quad \cdots \quad e^{jk(M-1)d\sin(\theta_i)}]^T$, where k and d represent the wave number and element spacing between radiating elements, respectively. As shown in Fig. 2, $\boldsymbol{\alpha} = [\alpha_1, \alpha_2, \cdots, \alpha_M]$ is an array response vector of the RX calibration signal injector ('calibration signal weight vector') and is measured before system installation. The calibration signal weight vector can be easily adjusted by controlling the length of the transmission line between the power divider and the coupler. The diagonal matrix is $\mathbf{H}_r = diag\{h_{r,1}, h_{r,2}, \cdots, h_{r,M}\}$ and each diagonal element represents a transfer function of the corresponding receiver.

The RX calibration coefficient estimator correlates the output snapshot $\mathbf{y}$ with the conjugated calibration signal to estimate the multi-channel transfer function $\hat{\mathbf{h}}_r$:

$$\hat{\mathbf{h}}_r = \Lambda^{-1} E\{\mathbf{y}(t)\, c^*(t)\}, \tag{4}$$

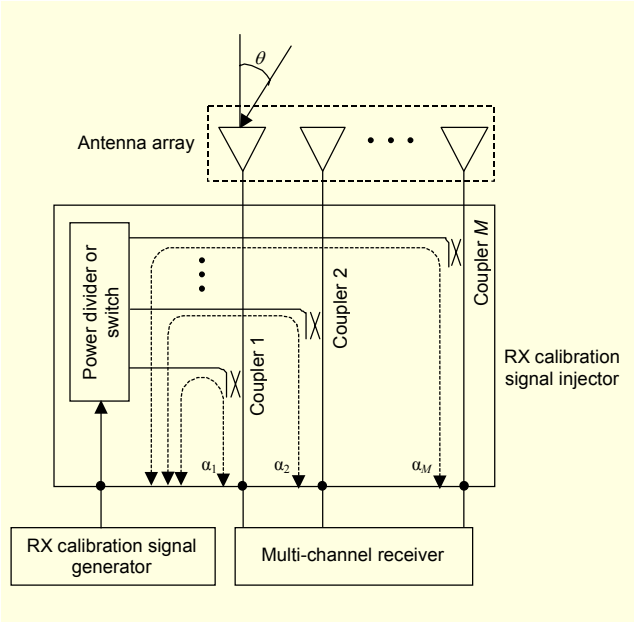

Fig. 2. RX calibration signal injector.

where $\hat{\mathbf{h}}_r = [\hat{h}_{r,1}, \hat{h}_{r,2}, \cdots, \hat{h}_{r,M}]^T$ denotes the multi-channel transfer function estimate consisting of a transfer function estimate of the *j*-th receiver, $\hat{h}_{r,j}$, and $\Lambda = diag\{\alpha_1, \alpha_2, \cdots, \alpha_M\}$ is a matrix representation of calibration signal weight vector $\boldsymbol{\alpha}$. The calibration coefficient matrix $\mathbf{C}_r$, an inverse of $\hat{\mathbf{H}}_r$, can be represented by

$$\mathbf{C}_r = diag\{\hat{h}_{r,1}^{-1}, \hat{h}_{r,2}^{-1}, \cdots, \hat{h}_{r,M}^{-1}\}. \quad (5)$$

The RX error corrector removes the transfer function by multiplying the received snapshot vector using the calibration coefficient matrix as follows:

$$\mathbf{z}(t) = \mathbf{C}_r \mathbf{y} \approx \sum_i \mathbf{a}(\theta_i) s_i(t) + \boldsymbol{\alpha} c(t). \quad (6)$$

To acquire a more accurate calibration coefficient, the calibration signal power, $\sigma_c^2 = E\{|c(t)|^2\}$, should be increased, which will also result in an increase in interference to the user signals $s_i(t)$. In CDMA basestation systems, a data sequence with small power and a long duration can be used as a calibration signal to reduce the interference. Nevertheless, it can still create interference to each user signal because the calibration signal power σ_p^2 might be larger than each user signal power $\sigma_{s,i}^2 = E\{|s_i(t)|^2\}$ when the capacity of the basestation is increased with the benefit of smart antennas. A method of reducing this interference is proposed in this paper.

The calibrated signals are distributed to *K* beamformers, and each beamformer performs spatial-filtering using weight vector $\boldsymbol{w}_i$. Provided that the transfer function error is removed perfectly, the user signal power to calibration signal power ratio at the *i*-th beamformer output is denoted by

$$\gamma_i = \frac{P_{s,i}}{P_c} = \frac{|\mathbf{w}_i^H \mathbf{a}(\theta_i)|^2}{|\mathbf{w}_i^H \boldsymbol{\alpha}|^2} \frac{\sigma_{s,i}^2}{\sigma_c^2}, \quad (7)$$

where $P_c = |\mathbf{w}_i^H \boldsymbol{\alpha}|^2 \sigma_c^2$ and $P_{s,i} = |\mathbf{w}_i^H \mathbf{a}(\theta_i)|^2 \sigma_{s,i}^2$ denote the residual calibration signal power and the signal power of the *i*-th user at the beamformer output, respectively. Note that the residual calibration signal power at the beamformer output is a function of the calibration signal weight vector as well as the calibration signal power. Since the user signals arrive at the basestation within a $\pm 60^o$ angular region, the beamforming weight $\boldsymbol{w}_i$ usually has a high correlation with the array response vectors for the angles within the sector angle region. Therefore, the residual calibration signal power will be reduced at the beamformer output if the calibration signal weight vector $\boldsymbol{\alpha}$ is chosen in such a way that it has a low correlation with the array response vectors for the angles within the sector angle region.

For the multi-channel transmitter calibration, a baseband calibration signal is injected into a multi-channel transmitter via a TX calibration signal injector. The baseband calibration signal is up-converted by a multi-channel transmitter to the RF frequency. A TX calibration signal extractor comprises a plurality of couplers and a switch, as shown in Fig. 3.

Each coupler extracts a small portion of the transmit signal energy from the corresponding transmitter. The switch connects one of the couplers to the TX calibration coefficient estimator. The TX calibration coefficient estimator down-converts and analyzes the RF transmit signal to estimate the transfer function of the selected transmitter. The process of

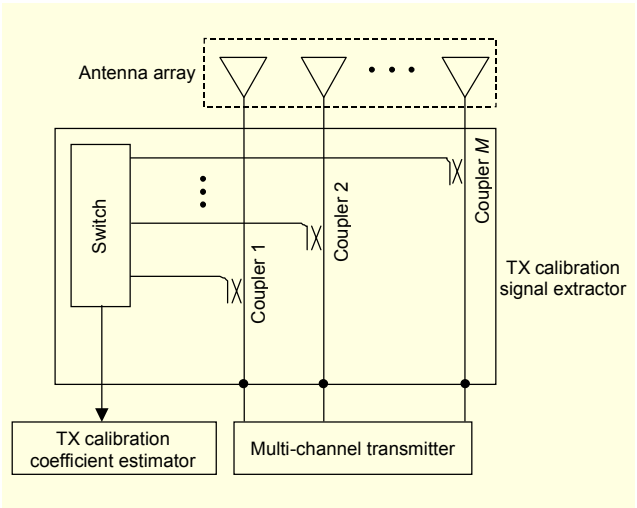

Fig. 3. TX calibration signal extractor.

estimating the transfer function, eliminating the array response of the TX calibration signal extractor and calculating the calibration coefficient, is similar with the multi-channel receiver calibration. The significant difference is that the multi-channel transmitter calibration does not suffer from noise in estimating the transfer function. Since all the user signals are spread by orthogonal codes in the downlink of CDMA communication systems, the calibration signal assigned by a specific orthogonal code is also orthogonal to all other user signals.

The simultaneous calibrations can be applied for the transmitter calibration if an M number of orthogonal codes are assigned to each transmitter. A sequential calibration using only one orthogonal code can also be successfully applied since the RF gain of the transmitter in the CDMA basestation system hardly changes; therefore the transfer function can be estimated by a calibration signal with a small power in a short time period. The digital transmit signal for each transmitter is multiplied by the corresponding calibration coefficient to correct the transfer function errors, thereby making the spatial signature of the RF transmit signal the same as the beamforming weight vector.

2. Computer Simulations

Figures 4(a) and 4(b) show the root mean square amplitude and phase errors for the transfer function estimate, respectively. The single frequency sinusoidal signal is used as a calibration signal. The x axis is the effective integration time, which is defined as the time divided by the period of the calibration sinusoidal signal. In the simulation, the calibration signal power to noise ratio is set to 0 dB. As expected, the root meat square errors become smaller as the integration time becomes longer.

Figure 5 shows the residual calibration signal power P_c at the beamformer output. It is assumed that the beamformer uses an array response vector of the user signal as a beamforming weight vector, $\mathbf{w}_i=\mathbf{a}(\theta_i)$. The solid and dashed lines are for the sequential calibration and simultaneous calibration, respectively. The number of radiating elements in the array, M, is set as 12, while the element spacing d is set as a 0.5 wavelength. The injected calibration signal power σ_c^2 for the simultaneous calibration is set to 1, where the calibration signal power for the sequential calibration is M times larger than that for the simultaneous calibration to compensate for the M times shorter integration time. The calibration signal weight vector is set to $\mathbf{e}=[1\ 0\ \ldots\ 0]^T$ for the sequential calibration. Thus, the residual power that does not depend on the beamforming weight vector at the beamformer can be calculated as

$$[P_c]_{dB} = 10\log_{10}\left(\left|\mathbf{w}_i^H\boldsymbol{\alpha}\right|^2\sigma_c^2\right)\Big|_{\substack{\boldsymbol{\alpha}=\mathbf{e},\\ \sigma_c^2=1}} \cong 10.8\ dB. \qquad (8)$$

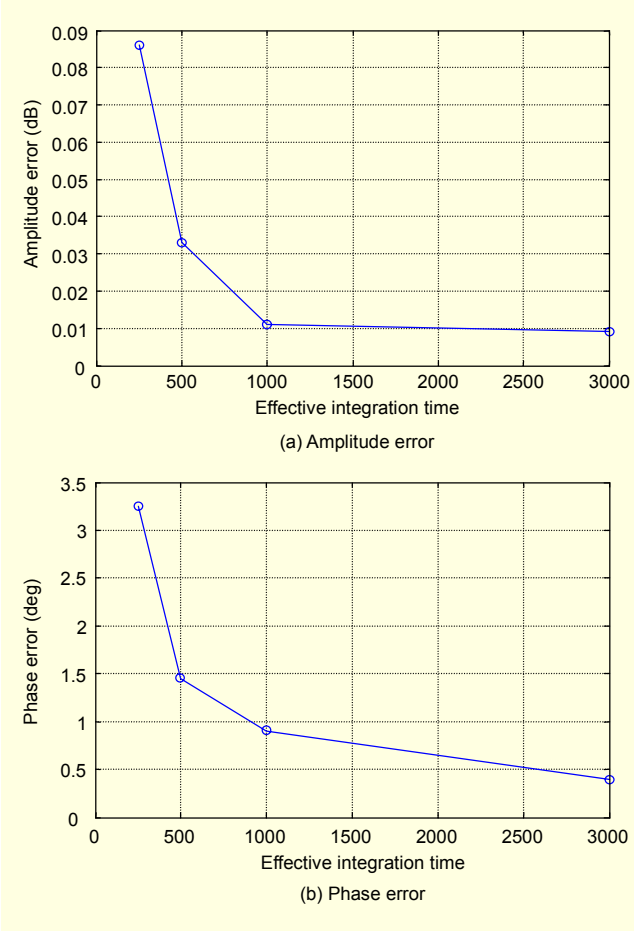

Fig. 4. Transfer function estimation error.

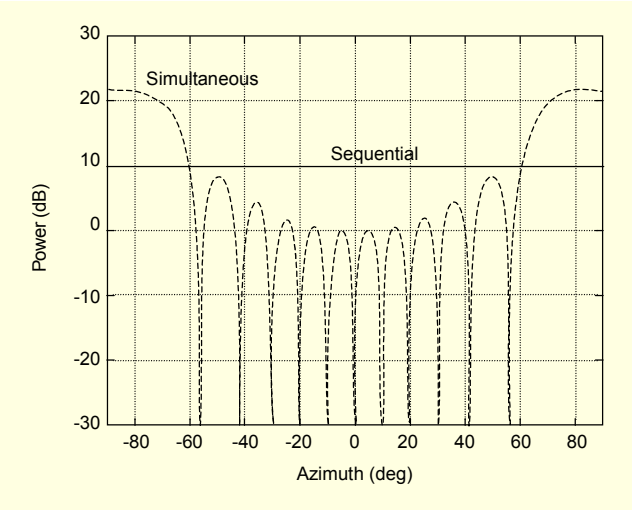

Fig. 5. Calibration signal power at the beamformer output ($\mathbf{w}_i=\mathbf{a}(\theta_i)$, $M=12$).

When the calibration signal weight vector $\boldsymbol{\alpha}$ is set to $\mathbf{a}(90°)$ for the simultaneous calibration, the residual calibration signal power can be expressed by

$$[P_c]_{dB} = 10\log_{10}\left(\left|\mathbf{w}_i^H \boldsymbol{\alpha}\right|^2 \sigma_c{}^2\right)\Big|_{\substack{\boldsymbol{\alpha}=\mathbf{a}(90^o),\\ \sigma_c^2=1}} = 20\log_{10}\{\mathbf{a}(\theta_i)^H \mathbf{a}(90^o)\}. \quad (9)$$

Figure 5 shows that the residual calibration signal power for the simultaneous calibration is smaller than that for the sequential calibration within the $\pm 60^o$ angular region.

III. Antenna Array Calibration

1. Model-Based Antenna Array Calibration

With the antenna array model, the array errors can be easily corrected by multiplying the transmit/receive data or weight vector by the inverse of the estimated error matrix. With error correction, all the elements in the array will have the same beam patterns, which is important for the sidelobe reduction in the beamforming and common downlink physical channels. In the CDMA basestation system, the common downlink physical channels such as the common pilot channels, paging channel and synchronization channel should be transmitted through an antenna beam without power fluctuations within the sector angle region. Therefore, if the element pattern fluctuates due to the mutual coupling error, an additional radiating element is needed for those channels. However, one of the radiating elements in the array can be used if the mutual coupling error is corrected.

The antenna array model is also useful for the smart antenna system requiring the measured array manifold for the AoA estimation. This is because the element patterns can be predicted from the array manifold measured at a small number of angles; the measurement time will then be significantly reduced in the mass production of the antenna array.

In this paper, a subspace optimization technique is used to overcome the limitations of the other algorithms proposed in [11], [12]. This technique estimates the error matrix **M** that minimizes the following cost function,

$$Q = \min_{\mathbf{M}} \sum_{i=1}^{N} \left\| (\mathbf{M}\mathbf{a}(\theta_i))^H \mathbf{U}_i \right\|^2, \quad (10)$$

where N denotes the number of angles at which the array response vectors are measured and $\mathbf{U}_i$ denotes a matrix whose column vectors are orthogonal to the measured array response vector $\mathbf{b}(\theta_i)$. We have

$$\mathbf{U}_i = [\mathbf{u}_{i,1}, \mathbf{u}_{i,1}, \ldots, \mathbf{u}_{i,N-1}], \quad \mathbf{b}(\theta_i) \perp \mathbf{u}_{i,j} \ (j = 1,2,\ldots,N-1), \quad (11)$$

where $\mathbf{u}_{i,j}$ (j=1, 2,…, N−1) can easily be calculated from the noise eigenvectors of matrix $\mathbf{R}_i = \mathbf{b}(\theta_i)\ \mathbf{b}(\theta_i)^H$. If the array response vector $\mathbf{b}(\theta_i)$ is measured in the antenna measurement range then the multipath signal power is small enough. In this case, the number of noise eigenvectors is N-1. Since the cost function utilizes the property of the vector orthogonality, it is not very sensitive to the isolated element pattern and/or center of the array. The optimum solution of (10) can be solved by finding the vector **m** that minimizes the cost function

$$Q = \mathbf{m}^H \left\{ \sum_{i=1}^{N} \left(\mathbf{A}_i^H \mathbf{U}_i \mathbf{U}_i^H \mathbf{A}_i \right) \right\} \mathbf{m}, \quad (12)$$

where **m** is a vector expression of the error matrix **M**, i.e., $\mathbf{M}\mathbf{a}_i = \mathbf{A}_i\mathbf{m}$. **M** can be any kind of matrix as well as the symmetric matrix assumed in [15]. Under the constraint of $[\mathbf{M}]_{1,1}=1$, the quadratic minimum of Q is

$$\mathbf{m} = \frac{\mathbf{G}^{-1}\mathbf{e}}{\mathbf{e}^H \mathbf{G}^{-1}\mathbf{e}}, \quad (13)$$

where $\mathbf{e} = [1\ 0 \ldots 0]^T$ and $\mathbf{G} = \sum_{i=1}^{N} \left(\mathbf{A}_i^H \mathbf{U}_i \mathbf{U}_i^H \mathbf{A}_i \right)$.

2. Computer Simulations

To evaluate the model-based antenna array calibration, an electromagnetic simulation was made for the microstrip antenna array with eight elements. All the antenna elements have about a 60^o half-power beam width and only the mutual coupling error is included. The spacing between radiating elements is a 0.47 wavelength, and the mutual coupling between the neighboring elements is −14 dB in the simulation. The length of the ground plate is assumed to be infinite.

Figure 6(a) shows the normalized element patterns calculated by electromagnetic simulation. The solid lines represent beam patterns for the left four elements and the dashed lines for the right four elements. Note that all the element patterns have fluctuations due to the mutual coupling. The array manifold for the angles, equally spaced from - 60° to 60° with 10° intervals, is used to estimate the mutual coupling matrix. Figure 6(b) shows the element patterns after error correction. The mutual coupling error was corrected by multiplying the measured array manifold **B** by an inverse of the estimated error matrix, $\hat{\mathbf{M}}^{-1}$. All the elements have the same beam patterns after error correction, which means that the antenna array model works very well when only the mutual coupling error is included.

Figure 7 shows the effect of a mutual coupling error on the beamforming. The antenna array is controlled to steer the 50° angle and a window is applied to reduce the sidelobe level. Figures 7(a) and 7(b) represent the array beam patterns without and with error correction. The dashed line represents the array

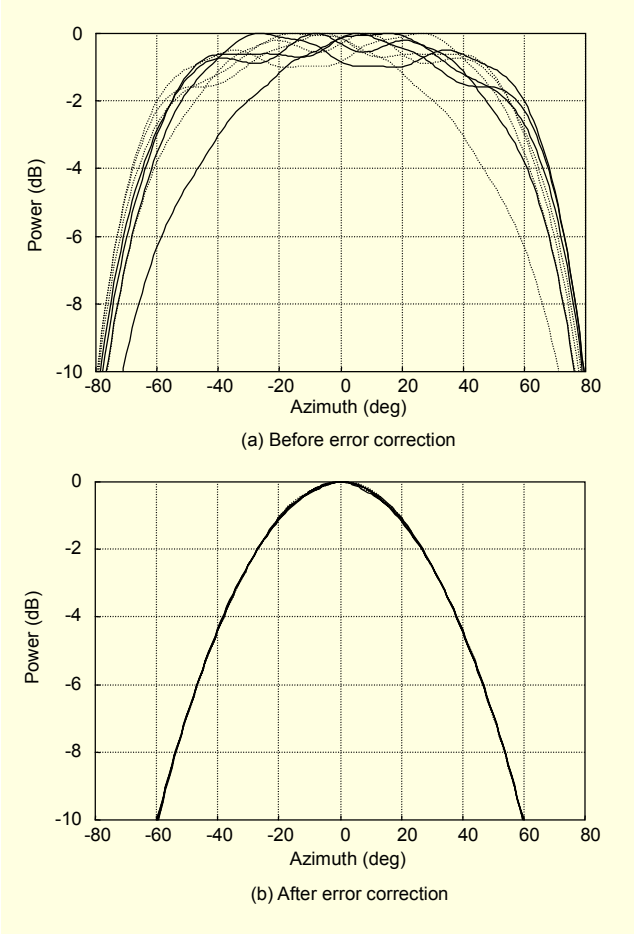

Fig. 6. Simulated element patterns.

beam pattern of the ideal antenna array $g_{ideal}(\theta)$ such that

$$g_{ideal}(\theta) = f(\theta)\ [\mathbf{\Lambda a}(45^\circ)]^H \mathbf{a}(\theta), \tag{14}$$

where $\mathbf{\Lambda}$ denotes the diagonal matrix whose diagonal terms denote the window value for the corresponding element and $f(\theta)$ is the isolated element pattern calculated from the simulation. The solid lines in Figs. 7(a) and 7(b) respectively represent the uncalibrated array beam pattern $g_{uncal}(\theta)$ and the calibrated array beam pattern $g_{cal}(\theta)$ such that

$$g_{uncal}(\theta) = [\mathbf{\Lambda a}(45^\circ)]^H \mathbf{b}(\theta) \tag{15}$$

and

$$g_{cal}(\theta) = \mathbf{w}_{cal}^H \mathbf{b}(\theta), \tag{16}$$

where $\mathbf{w}_{cal} = \{[\Lambda \mathbf{a}(45^\circ)]^H \hat{\mathbf{M}}^{-1}\}^H$ denotes the modified beamforming weight vector to correct the mutual coupling error. If the estimated mutual coupling matrix $\hat{\mathbf{M}}^{-1}$ is close to the true coupling matrix, the calibrated array pattern $g_{cal}(\theta)$ will be similar to the ideal array pattern according to the antenna array model in (1). Figure 7(a) shows that the uncalibrated array pattern has a relatively higher sidelobe compared to the ideal beam pattern, which will lead to higher interference to other user signals. However, Fig. 7(b) shows that the calibrated array pattern has almost the same beam pattern as the ideal one.

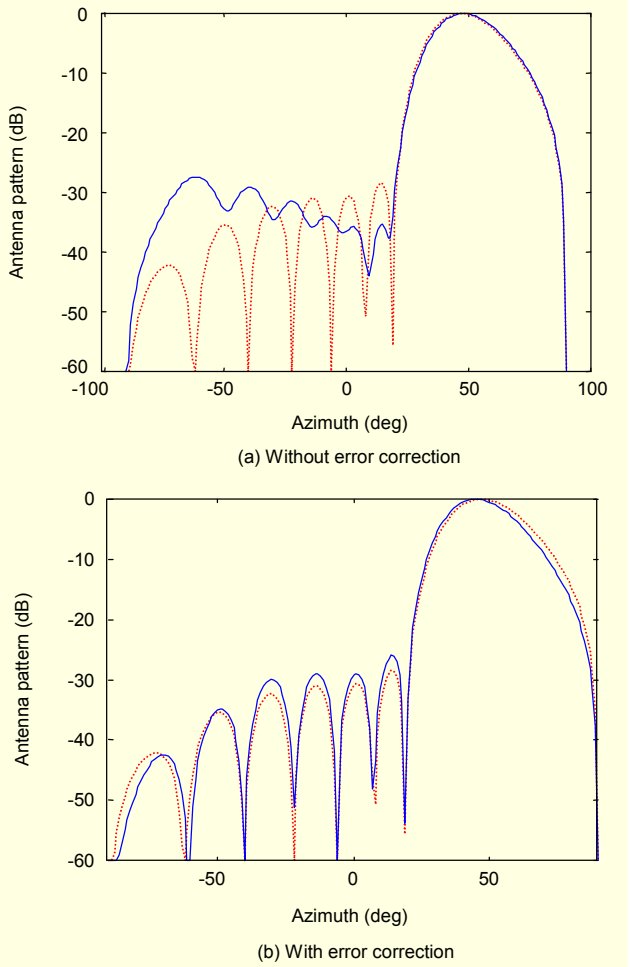

Fig. 7. Beam pattern of the antenna array steering at 50°.

3. Experiment Results

An experiment using a uniform linear array with eight printed dipole elements was conducted to evaluate the model-based antenna array calibration. The antenna array was built and measured using the ElectroScience Laboratory in Ohio State University. Figure 8 is a photograph of the printed dipole antenna array. The inter-element spacing is 5 cm and the aluminum ground plate is 40 cm wide and 24 cm high. No effort to reduce the edge scattering of the ground plate is made to investigate the effect of the modeling error.

Figure 9(a) shows the measured element patterns before error correction. The solid lines represent the beam patterns for

Fig. 8. Photograph of the printed dipole antenna array.

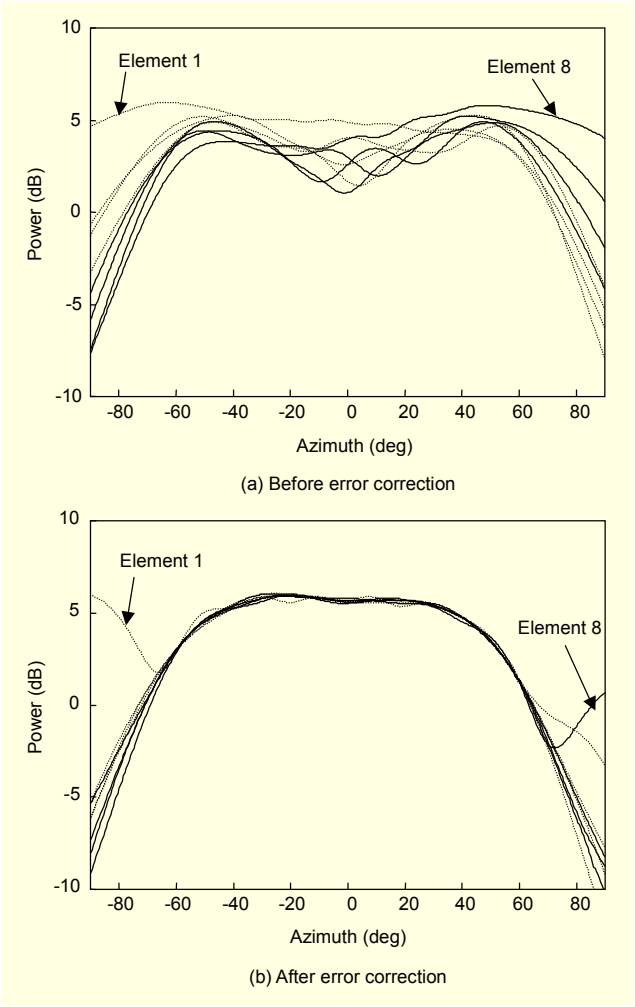

Fig. 9. Measured element patterns.

the left four elements and the dashed lines for the right four elements. Note that all the elements, especially the edge elements, have asymmetric patterns due to the edge scattering. The ripples in the patterns are mainly due to the mutual coupling. The measured array manifold for angles equally spaced from $-60°$ to $60°$ with $10°$ intervals is used to estimate the error matrix. Figure 9(b) shows the element patterns after error correction. Due to the modeling errors such as the edge scattering, the element patterns are somewhat different from each other for the angles outside the sector angle region. In particular, the first and eighth elements have significantly different patterns from those of the other elements, which is due to the fact that the edge scattering is more dominant for those elements. However, the pattern deviation is less than 0.5 dB within a $\pm 60^{o}$ angular region.

Figure 10 shows pattern prediction examples for the first and fourth antenna elements. The solid lines represent the measured patterns and the dotted lines the predicted patterns. The element patterns are predicted by the relationship in (1), in which the isolated element pattern $f(\theta)$ was assumed to be isotropic. In the case where the isolated element pattern is not isotropic, it can be estimated by averaging the calibrated element patterns, which are shown in Fig. 9(b). The prediction error for all elements in the array was less than 0.5 dB within the sector angle region in the experiment.

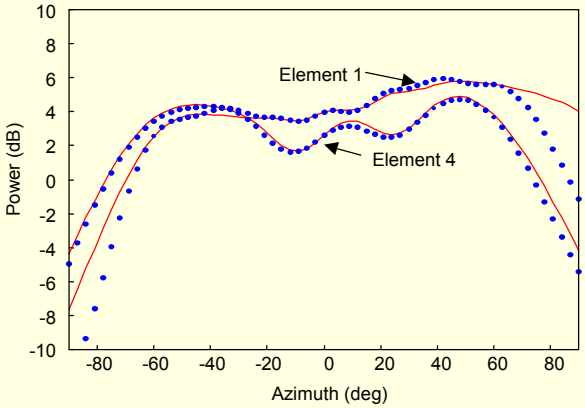

Fig. 10. Element pattern prediction.

IV. Conclusions

In this paper, array calibration algorithms to calibrate both the multi-channel RF transceiver and antenna array for the CDMA smart antenna system were investigated.

For the RF transceiver calibration, the structure of the multi-channel RF transceiver with the digital calibration apparatus and the calibration techniques were presented. A new RF receiver calibration scheme was proposed to reduce the residual calibration signal power at the beamformer. This residual signal power can be reduced by adjusting the calibration signal weight vector such that it has a low

correlation with the array response vectors of the user signals incoming to the antenna array. Due to the code orthogonality in the downlink, the multi-channel transmitter calibration does not suffer from the interference from the transmit user signals for the CDMA smart antenna system.

For the antenna array calibration, a model-based antenna array calibration was discussed to be applied for smart antenna systems using an electromagnetic simulation and experiment results. The experiment results showed that it works well within the sector angle region even in the presence of edge scattering. With the array calibration technique, all the elements had almost the same beam patterns and little power fluctuations. Therefore, one of the radiating elements in the antenna array can be used for transmitting the common downlink physical channels without using an additional radiating element. It was also shown that the element patterns can be predicted from the array response vectors measured at the small number of angles. In fact, this approach will be very useful for the mass production of the antenna array.

References

[1] Jack H. Winters, Jack Salz and Richard D. Gitlin, "The capacity of communication systems can be substantially increased by the use of antenna diversity," *Proc. ICUPC '92,* Sept. 1992, pp. 28-32.

[2] Joseph C. Liberti, Jr. and Theodore S. Rappaport, *Smart Antennas for Wireless Communications*: *IS-95 and Third Generation CDMA Applications*, Upper Saddle River, NJ : Prentice Hall, Inc, 1999.

[3] S. Tanaka, A. Harada, M. Sawahashi and F. Adachi, "Transmit diversity based on adaptive antenna array for W-CDMA forward link," *Proc. CIC '99* (*4th CDMA International Conference*), Sept. 1999, pp.282-286.

[4] Shiann-Shiun Jeng, Garret Toshio Okamoto, Guanghan Xu, Hsin-Piao Lin and Wolfhard J. Vogel, "Experimental evaluation of smart antenna system performance for wireless communications," *IEEE Trans. Antennas Propagat.*, vol. 46, no. 6, June 1998, pp. 749-757.

[5] K.R. Dandekar, H. Ling and G. Xu, "Effect of mutual coupling on direction finding in smart antenna applications," *IEE Electronics Letters*, vol. 36, no. 22, Oct. 2000, pp.1889-1891.

[6] Yosef Rockah and Peter M. Schultheiss, "Array shape calibration using sources in unknown locations – Part I: Far-field sources," *IEEE Trans. Acoust., Speech, Signal Processing,* vol. ASSP-35, no. 3, March 1987, pp. 286-299.

[7] Benjamin Friedlander and Anthony J. Weiss, "Eigenstructure methods for direction finding with sensor gain and phase uncertainties," *Proc. ICASSP '88*, April 1988, pp. 2681-2684.

[8] A. Paulraj and T. Kailath, "Direction of arrival estimation by eigenstructure methods with unknown sensor gain and phase," *Proc. ICASSP '85,* April 1985, pp. 640-643.

[9] Christian Passmann, Frank Hickel and Thomas Wixforth, "Investigation of a calibration concept for optimum performance of adaptive antenna systems," *Proc. VTC '98*, May 1998, pp. 577-580.

[10] S. Kobayakawa, M. Tsutsui and Y. Tanaka, "A blind calibration method for an adaptive array antenna in DS-CDMA systems using an MMSE algorithm," *Proc. VTC 2000-Spring*, Tokyo, May 2000, pp. 21-25.

[11] Hans Steyskal and Jeffery S. Herd, "Mutual coupling compensation in small array antenna," *IEEE Trans. Antennas Propagat.*, vol. 39, no. 12, Dec. 1990, pp. 1971-1975.

[12] J. Pierre and M. Kaveh, "Experimental performance of calibration and direction-finding algorithms," *Proc. ICASSP '91*, April 1991, pp. 1365-1368.

[13] I. J. Gupta, J. R. Baxter, S. W. Ellingson and H. G. Park, *An Experimental Study of Antenna Array Calibration*, Ohio State Univ. ElectroSci. Lab., Columbus, OH, Tech. Rep. 738600-3, March 2001.

[14] Lars Pettersson, Magnus Danestig, and U. Sjostrom "An experimental S-band digital beamforming antenna," *IEEE AES Systems Mag.,* Nov. 1997, pp. 19-27.

[15] I. S. D. Solomon, D. A. Gray, Yu. I. Abramovich and S. J. Anderson, "Performance of OTH radar array calibration," *Proc. ICASSP '98*, May 1998, pp. 2025-2028.

Mun Geon Kyeong received the BS and MS degrees in electronics engineering from Korea University, Seoul, Korea, in 1980 and 1985, and received the PhD degree in electrical engineering from Texas A&M University, Texas, USA, in 1993. Since joining Electronics and Telecommunications Research Institute (ETRI) in 1985, he has been engaged majorly in the research and development of communications transceivers and systems for various applications such as HF surveillance, ISDN-type electronic switching, IS-95/cdma-2000/WCDMA mobile radios, smart antenna beam-forming, and 4G broadband wireless packet access. His current research interest is largely centered on spectrum-efficient Hyper Multiple Access MC-CDMA 4G broadband mobile wireless transmission technology. From 1995 to 1999, he served as a Project/Team Manager for the FPLMTS foundational technologies research project, the CDMA cellular system research project. He also served as an Editor of ITU-R SG 8 TG 8/1 IMT-2000.RSPC-4 (on Terrestrial mobile BTS and Satellite Earth Station) for several years from 1995. From 2000 to 2002, as a Director he led a pioneering AMCD (Advanced Mobile Communication Department) research group of Radio & Broadcasting Research Laboratory, where he set up the research and development foundation of enhancement and breakthrough technologies for 3G+ and 4G mobile wireless communications in the areas of ultra high-speed packet data, All IP, TDD, MUD and smart antennas. Since 2002, he has been with Mobile Telecommunication Research Division as Principal Member of Research Staff. He has one commercialized world patent on universal signaling transceiver for electronic switching system. He has been listed in Who's Who in the World since 2000.

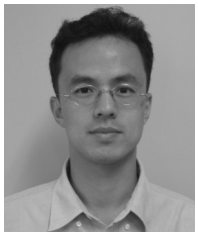

Hyung Geun Park received the BS and MS degrees in electronic engineering from Yonsei University, Seoul, Korea and Pohang University of Science and Technology (POSTECH), Pohang, Korea, in 1995 and 1997, respectively. Since 1999, he has been a Research Staff of Electronics and Telecommunications Research Institute (ETRI), Daejeon, Korea. His research interests include RF calibration and array signal processing for smart antenna systems.

Hyun Seo Oh received the BS degree in electronic engineering from Soongsil University, Seoul, Korea in 1982 and the MS degree in electronic engineering from Yonsei University, Seoul, Korea in 1985, and received the PhD degree in electronic engineering from Yonsei University, Seoul, Korea in 1998. Since 1982, he has been at Electronics and Telecommunications Research Institute (ETRI), now working as a Principal Member of Research Staff at Telematics Research Division of ETRI, Daejeon, Korea. He worked on the technical support for No.4 ESS operation and management, ASIC architecture and logic design of block and stream ciphering algorithm, and radio access technology development of IS-95 based digital cellular, PCS and IMT-2000 systems. He has joined ITS (Intelligent Transport Systems) project to develop 5.8 GHz DSRC packet communication system and smart antenna project to develop adaptive beamforming techniques for WCDMA cellular system and TDD-CDMA. Now he works for Telematics Communication Research Team as a Team Manager. His current research interests include radio access integration technology such as cellular, WLAN and terrestrial DMB for telematics services and inter-vehicle ad-hoc communication technology for anti-collision application.

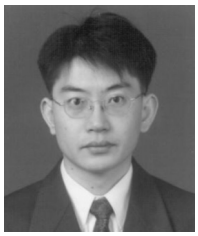

Jae-Ho Jung received the BS, MS, and PhD degrees in electronic engineering from Kyungpook National University, Daegu, Korea, in 1994, 1996, and 2004. Since 2000, he has been a Senior Research Staff of Electronics and Telecommunications Research Institute (ETRI), Daejeon, Korea. His research interests include wireless communication radio frequency system design, wave propagation theory and numerical antenna analysis.